Journal of Materials Chemistry C

ROYAL SOCIETY OF CHEMISTRY

COMMUNICATION

View Article Online
View Journal | View Issue

Cite this: J. Mater. Chem. C, 2022, 10, 14439

Received 14th July 2022,
Accepted 16th September 2022

DOI: 10.1039/d2tc02977d

rsc.li/materials-c

Functionalized anthrathienothiophenes: synthesis, properties, and integration into OFETs†

Garrett Fregoso, [a] Gehan S. Rupasinghe, [b] Maryam Shahi,[c] Karl Thorley,[c] Sean Parkin, [a] Alexandra F. Paterson [bc] and John Anthony *[ac]

For more than two decades, the silylethyne functionalization scheme has been used to induce strong π-stacking interactions in linear acenes and heteroacenes. As part of our efforts to better understand the crystal engineering aspects of silylethyne functionalization, along with an interest in studying the impact of ring topology on the electronic and optical properties of heteroacenes, we describe here the integration of thieno[3,2-*b*]thiophene (a non-linear isomer of the well-known anthradithiophene) into our well established crystal engineering scheme. By utilizing the thienothiophene moiety coupled with an asymmetric solubilizing group (isopropenyldiisopropylsilylethyne), we were able to achieve charge carrier mobilities (*μ*) upwards of 0.22 $cm^2 V^{-1} s^{-1}$. Based on their increased stability and promising initial mobilities, the use of this thienothiophene moiety may offer a new approach to the formation of larger heteroacene analogues with more than 5 aromatic rings.

Introduction

Since the development of TiPS pentacene,[1] silylethyne-substituted acenes and heteroacenes have become a desirable class of compounds for use in a variety of organic electronic devices as organic semiconductors (OSCs) due to their π-stacking interactions leading to strong electronic coupling, and their improved solubility that allow them to be easily processed into devices through cost effective, scalable methods.[1–8] The most successful of these chromophores have primarily consisted of linear, symmetric, aromatic cores such as acenes, acenedithiophenes, and aza-acenes.[1,9,10] The crystal engineering effects of silylethyne substitutions have been shown to follow well defined trends correlating crystal packing to the relative ratio between acene length and radius of the trialkylsilyl group.[1,11] As we push to better understand the crystal engineering effects of these substitutions, it is important to explore the impact of asymmetry of the chromophore on these well-established rules for tuning crystal packing. Additionally, these asymmetric cores may lead to altered photophysical properties and new crystal packing motifs, as well as overall improved stability of these materials. To address this issue, we aimed to modify the highly successful silylethyne-substituted anthradithiophene (ADT), first reported by Odom and co-workers (Fig. 1, left), where thiophene rings are fused to the central anthracene on both ends,[2] by preparing its constitutional isomer anthrathienothiophene (ATT), (Fig. 1, right) where both thiophenes are fused in sequence to only one side of the central anthracene, introducing asymmetry into the core. We aim to determine the impact of heterocycle asymmetry on our models for crystal packing as well as explore the changes to photophysical and electrochemical properties induced by the fused thienothiophene moiety.

Synthesis

The synthesis of the requisite anthrathienothiophene quinone **3** (Fig. 2) was adapted from work previously published by Katagiri and coworkers[12] with modifications to improve both yield and scalability of the synthesis. Most significant of these

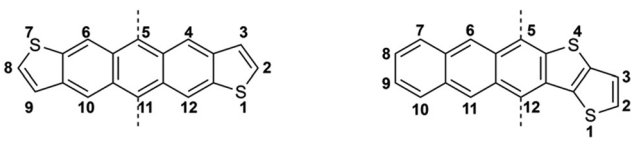

Fig. 1 Anthradithiophene (left) and anthrathienothiophene (right) aromatic cores with positional numbers notated. Dashed bonds indicate trialkylsilylethynyl functionalization positions.

[a] University of Kentucky, Department of Chemistry, Lexington, Kentucky 40506-0055, USA. E-mail: anthony@uky.edu
[b] University of Kentucky, Department of Chemical and Materials Engineering, Lexington, Kentucky, 40508, USA
[c] University of Kentucky Center for Applied Energy Research, Lexington, Kentucky 40511, USA

† Electronic supplementary information (ESI) available: Details of material characterization, methods of deice fabrication. Structures for F-iPDiPS ATT, diF-TiPS ATT, TiPS ATT, and F-TiPS ATT are filed with the CCDC under registry numbers 2181075–2181078. For ESI and crystallographic data in CIF or other electronic format see DOI: https://doi.org/10.1039/d2tc02977d

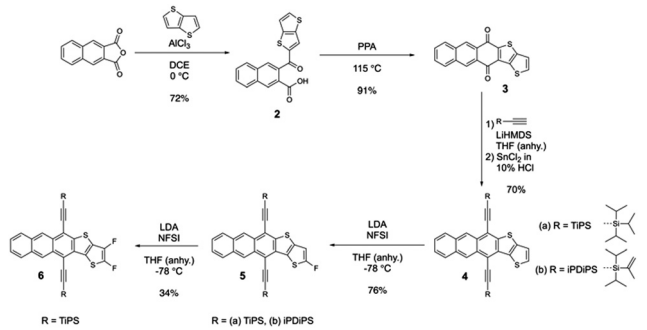

Fig. 2 Synthesis of trialkylsilylethynyl anthrathienothiophene and its fluorinated derivatives.

modifications were the elevation of temperature, and use of Soxhlet column extraction of the quinone (**3**). The derivatization with trialkylsilylethynyl groups at the 5,12-positions followed our usual methodology.[1] Once rearomatized, **4** was subjected to sequential fluorination to produce F-TiPS ATT (**5**), and DiF-TiPS ATT (**6**). Fluorine substitution on aromatic cores is ideal for crystal engineering due to the small atomic radius, stability, and electrostatic properties of fluorine.[13–18] It is also helpful because of the weak hydrogen bonding abilities of fluorine,[15,17,18] when compared with other hydrogen bond acceptors. Fluorine deviates from other halogens as it prefers C–F···H–C interactions over C–F···F–C interactions as the primary close contact.[13,15,16] Though the preference for C–F···F–C has been shown to be dependent on the abundance of fluorine within the structure, and the presence of fluorine across a symmetry center,[16] which should not be of concern with our asymmetric chromophore.

Crystal engineering

Molecules of unfluorinated ATT adopt a 1-D slipped-stack arrangement (Fig. 3a) wherein the silyl group blocks the π-surface of adjacent aromatic cores (Fig. 3a, middle), preventing any potential 2-D packing. Fluorine substitution on aromatic cores has been shown to convert 1-D packing to 2-D brickwork packing motifs in previously reported anthradithiophene systems through C–F···H–C and C–F···F–C interactions. Because of these patterns observed in symmetrical ADT systems, we wanted to explore the effect fluorination would have on this new asymmetric ATT core. Similar to ADT, mono- (2-) and di (2,3-) fluorination allows the ATT chromophore to adopt a crystal packing motif much closer to the traditional 2-D brickwork common in high performance transistor materials (Fig. 3b and c). The resulting C–F···H–C interactions help align the cores, enhancing π-stacking interactions and segregation of the chromophores from the solubilizing groups (Fig. 4).

Both mono- (2-) and di- (2-,3-)fluorinated derivatives of TiPS ATT adopt a "dimerized" brickwork packing motif, forming a bilayer of aromatic cores, wherein two layers adopt well organized 2-dimensional packing, but are then offset along the short axis from the adjacent bilayer. We aimed to make a minute change to trialkylsilyl group in an effort to nudge the

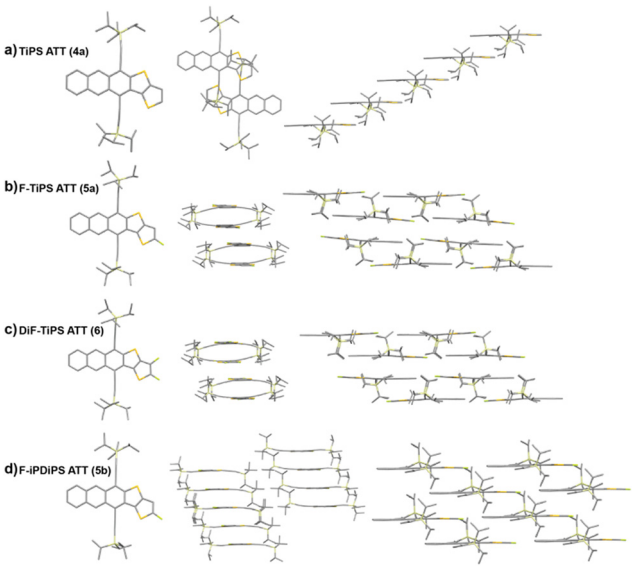

Fig. 3 Crystal structures and packing for (a) TiPS ATT (**4a**), (b) F-TiPS ATT (**5a**), (c) DiF-TiPS ATT (**6**), and F-iPDiPS (**5b**). Hydrogens have been omitted for clarity.

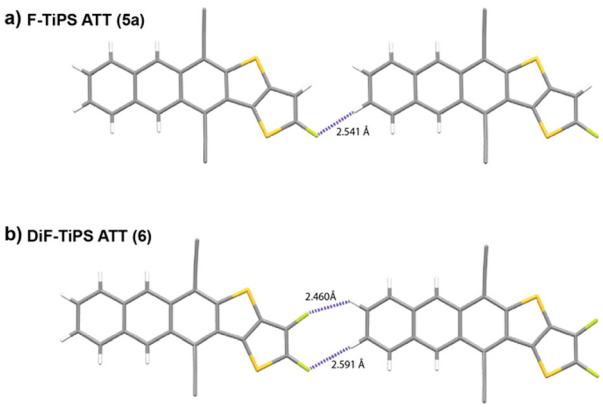

Fig. 4 Close contacts present between chromophores for (a) F-TiPS ATT (**5a**) and (b) DiF-TiPS ATT (**6**). Trialkylsilyl groups omitted for clarity.

packing towards a more regular 2-D brickwork packing. To satisfy this condition, we utilized isopropenyldiisopropylsilylethynyl solubilizing group (iPDiPS). Use of this iPDiPS group allowed us to make the smallest possible change to the solubilizing group, a total difference of four hydrogens between TiPS and iPDiPS. The loss of these hydrogens resulted in an increase of 0.83 Å^3 to the calculated volume (Table 1) of the solubilizing group, enough to allow F-iPDiPS ATT (**5b**) to adopt a more traditional 2-D brickwork packing motif (Fig. 3d).

Table 1 Calculated volume and surface area for trialkylsilyl solubilizing groups

	Volume (Å^3)	Surface area (Å^2)
TiPS (**a**)	199.54	216.77
iPDiPS (**b**)	200.37	218.53

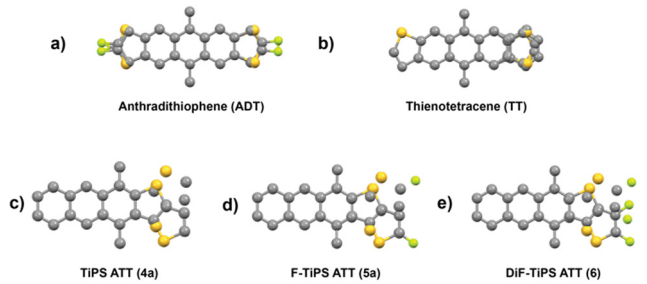

Fig. 5 Crystal structures, including disorder, for (a) F-TES ADT, (b) TiPS TT,[9] (c) TiPS ATT (**4a**), (d) F-TiPS ATT (**5a**), and (e) DiF-TiPS ATT (**6**). Solubilizing groups and hydrogens have been removed for clarity.

Unlike other dithiophene systems such as ADT, and other asymmetric systems like thienotetracene (TT),[9] ATT exhibits a lower degree of thiophene disorder within the crystal (Fig. 5). ADT is routinely synthesized as an inseparable mixture of *syn*- and *anti*-isomers[2,19,20] which causes a substantial degree of disorder in the lattice. The combination of isomerism and long and short axis ring flips causes the sulfur atoms to be distributed across four corners of the aromatic backbone in a 1 : 1 : 1 : 1 ratio. Thienotetracene also experiences a similar distribution of the sulfur atom resulting from ring flips across the long and short axes with the sulfur also presenting in the four corners of the backbone in a 1 : 1 : 1 : 1 ratio. Conversely, our ATT compounds showed no observable long axis ring flip, and exhibit a very small amount of short axis ring flip, with observed ring flip ratios of 95.2 : 4.8, 97.4 : 2.6, and 94.5 : 5.5 for TiPS (**4a**), F-TiPS (**5a**), and DiF-TiPS (**6**) respectively (Fig. 5).

Transfer integrals were calculated for the fluorinated derivatives of TiPS and iPDiPS ATT, utilizing tuned ωB97XD/6-31G* with chloroform PCM. For F-TiPS ATT, which adopts a "dimerized" brickwork packing motif, we observe fairly homogenous intradimer couplings as well as strong interdimer couplings (Fig. 6a) which implies that the slip that occurs between the brickwork bilayers does not break the 2-D nature of brickwork packing. Crystal packing with the iPDiPS solubilizing group eliminated the bilayer slip, and we observe smaller but more symmetrical couplings in the calculated transfer integrals (Fig. 6b).

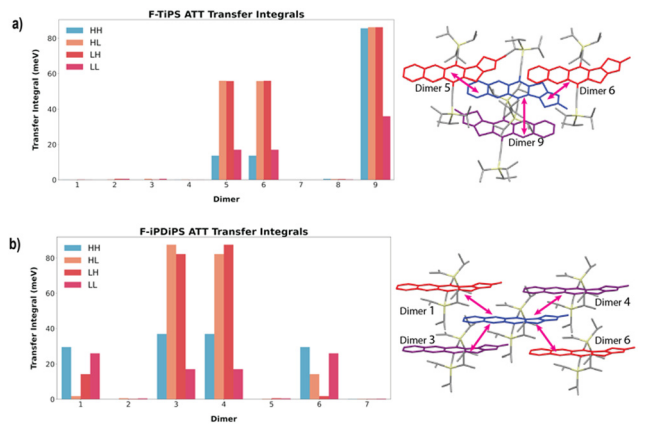

Fig. 6 Calculated transfer integrals describing HOMO–HOMO (HH), HOMO–LUMO (HL), LUMO–HOMO (LH) and LUMO–LUMO (LL) interactions for (a) F-TiPS ATT (**5a**), and (b) F-iPDiPS ATT (**5b**) calculated using tuned ωB97XD/6-31G* with chloroform PCM, corresponding dimers are notated on the right.

Device studies

Organic thin-film transistor (OTFT) devices were fabricated in a top-gate, bottom-contact geometry on Borofloat glass substrates. 40 nm gold electrodes were deposited *via* vacuum deposition, through a shadow mask, to pattern source/drain electrodes with channel lengths varying from 30–100 μm, and then treated with pentafluoro benzenethiol. Materials were deposited through two-step spin coating at a concentration of 10 mg mL^{-1} in chlorobenzene, spinning first at 500 rpm for 10 s followed by spinning at 1000 rpm for 30 s. The thin-films were then annealed at 100 °C for 5 min. Pristine CYTOP CTL-809M dielectric was also deposited *via* two-step spin coating; 500 rpm for 10 s followed by 2000 rpm for 30 s. The Cytop film thickness was measured using a Dektak profilometer yielding a

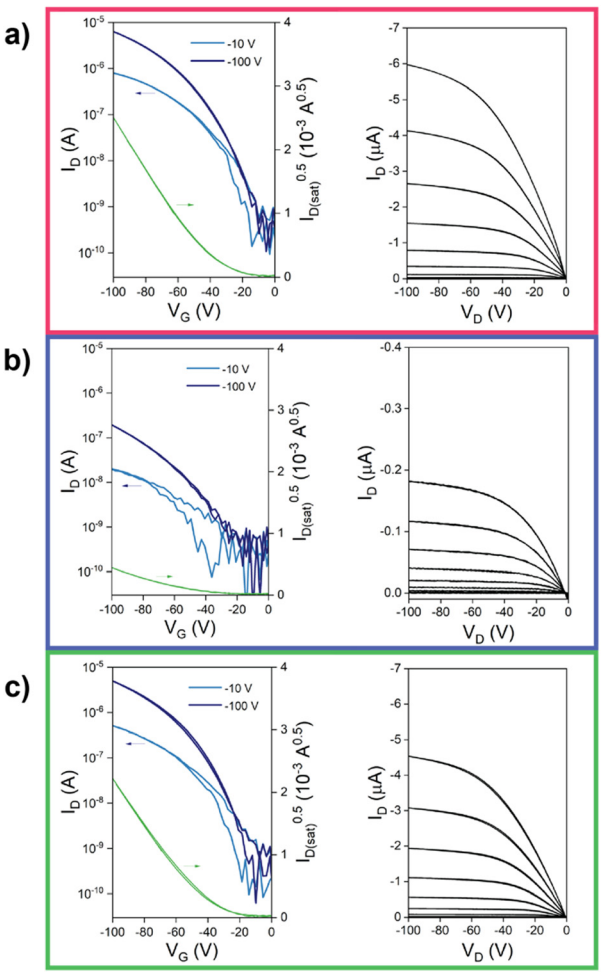

Fig. 7 Transistor data for best performing devices for (a) F-TiPS ATT (**5a**) (b) DiF-TiPS ATT (**6**) and (c) F-iPDiPS ATT (**5b**) showing transfer characteristics (left) and output characteristics (right). Representative devices have a channel length and width of 100 μm and 1000 μm, respectively.

Table 2 Device characteristics for devices made from fluorinated ATT derivatives that exhibited 2-D crystal packing geometries

	μ_{max} ($cm^2\ V^{-1}\ s^{-1}$)	μ_{avg} ($cm^2\ V^{-1}\ s^{-1}$)	$I_{on/off}$
F-TiPS ATT (**5a**)	0.224	0.139	10^4
DiF-TiPS ATT (**6**)	0.011	0.007	10^2
F-iPDiPS ATT (**5b**)	0.178	0.134	10^4

film thickness of 1326.8 nm with a capacitance of 1.4×10^{-9} F cm^2. Devices were then annealed at 50 °C for 60 min (none of these molecules showed any phase transitions below 190 °C), before deposition of a 100 nm thick aluminium gate. Device outputs are shown in Fig. 7.

Out of the three materials, we find F-TiPS ATT exhibits the highest maximum hole mobility, at 0.224 $cm^2\ V^{-1}\ s^{-1}$. This is significantly greater than previously reported for non-ethynylated ATTs, where mobilities are on the order of 10^{-2}, in devices processed in the same way (spin-coated).[12] Additionally, the average values shown in Table 2 are taken from 5 devices across a broad range of channel lengths (30 to 100 μm – device statistics and mobility spread are presented in Fig. S3, ESI†). We observed improved performance and higher mobilities with the longest channel length devices for all three material systems. Along with the linearity of $\sqrt{I_D}$ with respect to gate voltage, this suggests the devices likely suffer from a contact resistance that can result in an underestimated measured mobility. The average values reported here are therefore a conservative estimate and, along with the fact the mobilities are significantly greater than previously reported non-ethynylated ATTs, indicate excellent potential for future optimization, from both crystal packing and device optimization standpoints.

Optical and electronic studies

While these novel anthrathienothiophenes are constitutional isomers of anthradithiophenes they exhibit considerably different optical, photostability, and electronic properties (Fig. 8 and Table 3). Fluorination of the 2- and 3-positions does not induce the characteristic absorption blue-shift observed in other fluorinated acenes and heteroacenes, implying the additional annulated thiophene behaves more like an isolated double bond rather than an additional aromatic ring, buffering the aromatic core from the impact of substitution at the 2-, and 3-positions. This property allowed us to modify the periphery in order to drive crystal packing while not fundamentally altering the electronic environment of the aromatic core.

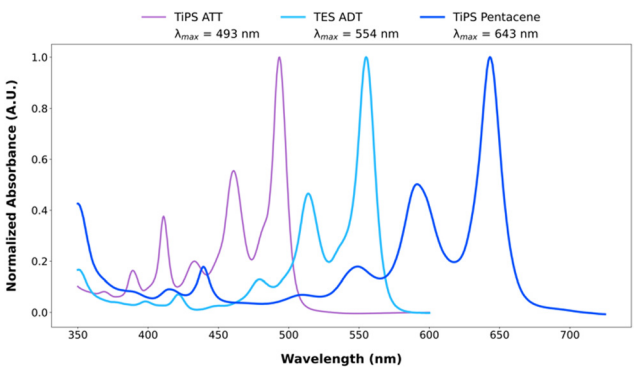

Fig. 8 Observed blue-shifted absorbance of anthrathienothiophenes compared to analogous 5-ring aromatic and heteroaromatic systems. Spectra were taken in toluene at a concentration of 50 μM. We saw no evidence of aggregation-induced peak broadening even at higher concentrations.

Table 3 Measured optical and electrochemical values for various ATT derivatives compared to F-TES ADT

	TiPS ATT (**4a**)	F-TiPS ATT (**5a**)	DiF-TiPS ATT (**6a**)	F-TES ADT
λ_{max} (nm)	493	493	491	525
E_{opt} (eV)	2.49	2.49	2.49	2.31
E_{ox} (meV)	624	638	718	564

CV were run in 0.1 M $Bu_4NH_4PF_6$ in DCM with glassy carbon working, Ag counter, and Ag/AgCl in 3 M NaCl reference electrodes and E_{Ox} is referenced to Fc/Fc^+ for each compound. Absorbance and emission spectra were run in toluene at a concentration of 50 μM, and E_{opt} is estimated from the intersection point of the absorbance and emission traces.

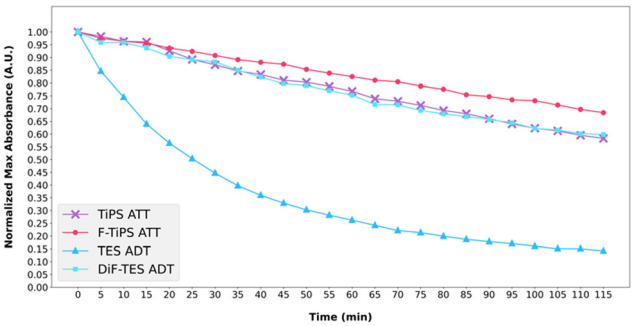

Fig. 9 Comparative stability study of ATTs *vs.* ADTs under constant 350 nm irradiation over 2 hours. Solutions were prepared in toluene at an approximate concentration of 50 μM for each compound.

By moving the alkyne substitution position closer to the heterocycle, we observed a considerable increase in photostability for unfluorinated ATT compared to other unfluorinated 5-ring heteroacenes (Fig. 9). This enhanced stability is likely due to there being no additional Clar sextets formed through the primary acene decomposition route with singlet oxygen. Since the outer thiophene appears to buffer the core from the 2-, and 3-positions, we observed a nominal increase in photostability induced by fluorinating the core. While the optical properties of the ATTs reported herein remain consistent, the electronic properties better show the effects of successive fluorination at the 2- and 3-positions through induction.

Conclusions

The use of the thienothiophene moiety has offered a new route for the development of heteroacene analogues to the extended acenes. The ability to fine tune the solid-state properties of these compounds through strategic derivatization of a common

aromatic core, while not drastically changing the optical and electronic characteristics, has allowed us to systematically alter the crystal packing and control the π-surface overlap leading to competitive charge carrier mobilities for F-TiPS ATT and F-iPDiPS ATT. However, fluorination at the 3-position induced a larger change in the HOMO of the core leading to poor charge injection and reduced mobility. While the mobilities reported herein leave room for growth, they do represent improvement over previously reported mobilities for comparable non-ethynylated ATTs, and with further material and device optimization, we expect to see further improvements in charge carrier mobility.

Conflicts of interest

There are no conflicts to declare.

Acknowledgements

This material is based upon work supported by the National Science Foundation under Cooperative Agreement No. 1849213. Any opinions, findings, and conclusions or recommendations expressed in this material are those of the author(s) and do not necessarily reflect the views of the National Science Foundation.

Notes and references

1 J. E. Anthony, D. L. Eaton and S. R. Parkin, *Org. Lett.*, 2002, **4**, 15–18.
2 M. M. Payne, S. A. Odom, S. R. Parkin and J. E. Anthony, *Org. Lett.*, 2004, **6**, 3325–3328.
3 J. E. Anthony, *Angew. Chem., Int. Ed.*, 2008, **47**, 452–483.
4 B. Purushothaman, S. R. Parkin and J. E. Anthony, *Org. Lett.*, 2010, **12**, 2060–2063.
5 M. M. Payne, S. R. Parkin and J. E. Anthony, *J. Am. Chem. Soc.*, 2005, **127**, 8028–8029.
6 M. Berggren, D. Nilsson and N. D. Robinson, *Nat. Mater.*, 2007, **6**, 3–5.
7 A. C. Arias, J. D. MacKenzie, I. McCulloch, J. Rivnay and A. Salleo, *Chem. Rev.*, 2010, **110**, 3–24.
8 C. Reese, M. Roberts, M. M. Ling and Z. Bao, *Mater. Today*, 2004, **7**, 20–27.
9 M. L. Tang, A. D. Reichardt, T. Siegrist, S. C. B. Mannsfeld and Z. Bao, *Chem. Mater.*, 2008, **20**, 4669–4676.
10 B. Wex, O. El-Ballouli, A. Vanvooren, U. Zschieschang, H. Klauk, J. A. Krause, J. Cornil and B. R. Kaafarani, *J. Mol. Struct.*, 2015, **1093**, 144–149.
11 B. D. Rose, P. J. Santa Maria, A. G. Fix, C. L. Vonnegut, L. N. Zakharov, S. R. Parkin and M. M. Haley, *Beilstein J. Org. Chem.*, 2014, **10**, 2122–2130.
12 Y. Ogawa, K. Yamamoto, C. Miura, S. Tamura, M. Saito, M. Mamada, D. Kumaki, S. Tokito and H. Katagiri, *ACS Appl. Mater. Interfaces*, 2017, **9**, 9902–9909.
13 A. R. Choudhury and T. N. Guru Row, *Cryst. Growth Des.*, 2004, **4**, 47–52.
14 Y. Lee, S. Ryu, E. Choi, D. Ho, T. Earmme, C. Kim and S. Y. Seo, *Synth. Met.*, 2021, **282**, 116944.
15 P. Panini and D. Chopra, Understanding of Noncovalent Interactions Involving Organic Fluorine, in *Hydrogen Bonded Supramolecular Structures*, ed. Z.-T. Li and L.-Z. Wu, Springer, Berlin Heidelberg, 2015, pp. 37–67.
16 D. Chopra and T. N. G. Row, *CrystEngComm*, 2011, **13**, 2175–2186.
17 P. A. Champagne, J. Desroches and J. F. Paquin, *Synthesis*, 2015, 306–322.
18 E. O. Levina, I. Y. Chernyshov, A. P. Voronin, L. N. Alekseiko, A. I. Stash and M. v Vener, *RSC Adv.*, 2019, **9**, 12520–12537.
19 J. G. Laquindanum, H. E. Katz and A. J. Lovinger, *J. Am. Chem. Soc.*, 1998, **120**, 664–672.
20 M. M. Payne, S. R. Parkin, J. E. Anthony, C. C. Kuo and T. N. Jackson, *J. Am. Chem. Soc.*, 2005, **127**, 4986–4987.